Received: 30 June 2020 | Revised: 26 January 2021 | Accepted: 5 February 2021

IET Image Processing

DOI: 10.1049/ipr2.12166

The Institution of Engineering and Technology WILEY

ORIGINAL RESEARCH PAPER

Towards accurate classification of skin cancer from dermatology images

Anjali Gautam[1] | **Balasubramanian Raman**[2]

[1] Department of Information Technology, Indian Institute of Information Technology, Allahabad, Prayagraj, Uttar Pradesh, India

[2] Department of Computer Science and Engineering, Indian Institute of Technology Roorkee, Roorkee, Uttarakhand, India
(Email: bala@cs.iitr.ac.in)

Correspondence
Anjali Gautam, Department of Information Technology, Indian Institute of Information Technology, Allahabad, Prayagraj, Uttar Pradesh, India.
Email: anjaligautam@iiita.ac.in

Abstract

Skin cancer is the most well-known disease found in the individuals who are exposed to the Sun's ultra-violet (UV) radiations. It is identified when skin tissues on the epidermis grow in an uncontrolled manner and appears to be of different colour than the normal skin tissues. This paper focuses on predicting the class of dermascopic images as benign and malignant. A new feature extraction method has been proposed to carry out this work which can extract relevant features from image texture. Local and gradient information from x and y directions of images has been utilized for feature extraction. After that images are classified using machine learning algorithms by using those extracted features. The efficacy of the proposed feature extraction method has been proved by conducting several experiments on the publicly available image dataset 2016 International Skin Imaging Collaboration (ISIC 2016). The classification results obtained by the method are also compared with state-of-the-art feature extraction methods which show that it performs better than others. The evaluation criteria used to obtain the results are accuracy, true positive rate (TPR) and false positive rate (FPR) where TPR and FPR are used for generating receiver operating characteristic curves.

1 | INTRODUCTION

Skin cancer—the most commonly found disease around the globe which occurs when the skin is exposed to the Sun's UV rays [4]. Some other risk factors also include smoking, old age, family history and so forth. UV rays change the DNA structure of the epidermis and the region which is affected by these rays forms spot on the skin whose colour differ from the surrounding normal skin colour. These affected skin cells grow rapidly and also depends person to person and its type. The number of skin cancer cases is increasing everyday as per the records of the world health organization (WHO) [3] and study also indicates that it has also become principal causes of the patient's death. Skin cancer is broadly categorized into two types, that is benign and malignant. Benign is the initial phase of skin cancer, which if detected in early stages can be easily cured otherwise they become malignant. Skin tissues which are malignant categorized into melanoma, nodular melanoma, basal cell carcinoma (BCC) and squamous cell carcinoma [8, 20, 29]. These malignant tissues are identified as most generally occurring and threatening cancer. Therefore, if they are treated in time patient's life can be saved.

The information given by the WHO shows that from last decades there have been a drastic increase in the cases of skin cancer. It is observed that every year 2 to 3 million cases globally belongs to non-melanoma cases; however, due to melanoma approximately 1,32,000 cases have been observed [3]. This shows that due to the thinning of the ozone layer the number of skin cancer patients is also increasing as it protects us from harmful UV radiations of the sun. According to the study, if the ozone layer is depleted by 10%, then there will be an increase of 3 lakh non-melanoma cases and 45 hundred melanoma cases [2]. In India, Globocan 2018 [1], an online source, shows that non-melanoma cases increased to 11,57,294 whereas 7,84,821 people died due to the emergence of this deadly disease. However, if focus is given to only melanoma skin cancer, then the number of cases accounts for 0.26% of all cancer cases and due to this, the number of deaths is 2053 which is also 0.26%. For the 5-year prevalence (all ages), it is identified that the percentage of skin cancer counts increased from 0.26% to 0.54%. Thus,

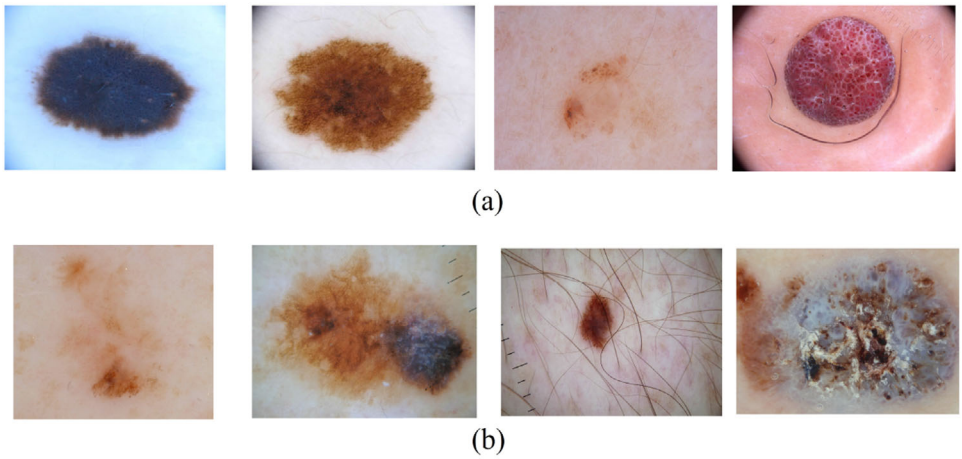

FIGURE 1 Selected images of (a) benign and (b) malignant skin cancer from ISIC 2016 dataset

it is very important that patients should be given appropriate medical treatment.

Dermoscopy images have taken part in a remarkable responsibility of improving the viability rate of patients by helping them in early prognosis of disease. Computer-aided diagnosis (CAD) systems can assist physicians in making right decisions for lesion boundary detection, useful features extraction and classification tasks and so forth [14, 27]. Dermoscopy technique, also known as epiluminescence microscopy (ELM), dermatoscopy or surface skin microscopy, is used by dermatologists for skin cancer diagnosis. It is performed by expert dermatologists by rubbing gel onto the surface of skin lesion, thereafter, dermatoscope digital imaging systems are used to obtain enlarged images with the improved colour combination. This helps in identifying the pattern and structure of the lesion more accurately. There are several methods which are used for the diagnosis of melanoma, such as seven-point checklist [18], ABCD (asymmetry, border irregularity, colour and dermoscopic structure) [22] and ABCDE (asymmetry, border, colour, diameter and evolution) [37].

In addition to the clinical approach, there are several technical challenges faced by clinicians as well as researchers to identify skin cancer. The biggest challenge is skin tone, if the cancer detection model is based on an image dataset of a particular region like USA (those with white skin) then there is a possibility of not achieving the desired results when tested with dark skin tone images (persons living in area having highest UV radiations (like Africa and South Asia)). Therefore, it is very important to have images of all skin tones in the dermatology image dataset that can be used to obtain more accurate results. One of the other technical challenges for researchers is the variation in image quality, as of being captured with different settings of skin capturing device. Sometimes there are situations where images are of different sizes and to make them of the same size, quality needs to be compromised. This is mostly seen in the case of deep learning based models, where all the images being fed to the system need to be of same size. Therefore, to create a running model, we sometimes need to reduce the size of the images by 10% from their original size. Challenges are not limited to such as it is very difficult to find labelled data in medical practice. Computational expenses for identifying cancer from images are high as cancerous lesions have infinite patterns. Extraction of high quality features are also required for better results. Therefore, to overcome these issues, research in this area has taken a boom.

Our contributions: In this article, our contributions to classify dermatology images of skin cancer in International Skin Imaging Collaboration (ISIC) 2016 challenge dataset (or International Symposium on Biomedical Imaging (ISBI) 2016 dataset) into two classes, that is benign and malignant, whose sample images are depicted in Figure 1 are as follows:

1. We have proposed a new feature extraction method named as a Regional Information Pattern (ReIP) for extracting useful regional information from the local neighbourhood of image pixels. The information related to changes in the intensity level of image pixels and details of how much the adjacent neighbour of a pixel is different from it.
2. Extracted features which are in the form of the 1-D feature vector are then fed to the classification algorithm for better results.
3. Several experiments have been conducted for proving that our ReIP features give better classification results as compared to other methods. Experiments are based on classification of extracting features by using linear Support Vector Machine (SVM), medium k Nearest Neighbour (kNN), ensemble bagged trees and ensemble boosted trees.

For image classification, feature set is required to be fed to the classifier. Therefore, it is very important to extract meaningful features from the images especially those corresponds to required detail. The main motivation to propose ReIP method here is to extract information from the neighbourhood of center image pixel and adjacent neighbourhoods. Extracted information is also based on the change in the intensity of neighbourhood pixels and for this we have used the gradient concept. As the method is extracting regional information from images, we have named it as Regional Information Pattern (ReIP) and it

is also mentioned in point 1 of contribution. Previous descriptors are unable to extracted very negligible (i.e. pattern of all neighbouring pixels) information. However, ReIP is able to easily identify patterns from an image by performing some calculations. The concept of extracting information from the neighbours of neighbour have not been used by previous methods as they have only focused on extracting neighbourhood information of center pixels; which is not satisfiable as cancer can be of any shape, size and pattern. Our method ReIP finds very deep information from images in such a way that normal skin pixels do not have any neighbourhood property of cancer pixels. Therefore, it helps in giving better classification results as compared to others.

The remaining structure of this article is given as: in Section 2 previous work is presented, background preliminaries in Section 3, feature extraction and classification methodology of this paper have been discussed in Section 4, details of ISIC 2016 dataset and conducted experiments are given in Section 5, discussion is presented in Section 6 and the conclusion of whole article is given in Section 7.

2 | RELATED WORK

Skin cancer is widely spread in the worldwide and thus it requires researchers to focus on this field. CAD system has been designed by researchers for the diagnosis of skin cancer by using several techniques. Semi-automatic and automatic methods are developed for segmentation and classification of skin cancer. Segmentation refers to the identification of a region of interest and classification means to predict the class to which object refers like benign and malignant for skin cancer or in other types as discussed in Section 1.

Marchetti et al. [26] have published their work on the comparative analysis of results obtained by different researcher who have worked on ISIC 2016 of ISBI. This dataset contains dermoscopic images of skin lesions which belong to either benign or malignant case. On this dataset, the research is still going on in order to increase the segmentation and classification accuracy. Wu et al. [45] proposed the method which can automatically identify correct skin lesion boundary. They have used Otsu's thresholding [33] followed by affinity propagation clustering and simple linear iterative clustering (SLIC) method. At last, to segment the lesion boundary they used supervised learning method. Yuan et al. [50] have also worked on automatic segmentation where they used 19-layer deep convolutional neural networks (CNNs) with Jaccard distance. Jafari et al. [19] work was based on deep neural networks where an effective selection of training patches was more effective in the detection of a lesion's border. Al-masni et al. [6] have proposed full resolution convolutional networks (FrCN) for the segmentation of lesions. Their FrCN does not require any pre- or post-processing of images and directly learns the full resolution features of each individual pixel. Li et al. [23] proposed a dense deconvolutional network (DDN) which has a ground of residual learning. Their method also does not require any pre- or post-processing in order to segment lesion boundary. Dash et al. [9] proposed an automated method for psoriasis lesion segmentation by utilizing the modified architecture of U-Net, known as PsLSNet. PsLSNet is 29-layer deep fully CNN, which automatically extracts spatial information. Their method also provides accelerated training by reducing the covariate shift by the implementation of batch normalization. Xie et al. [47] proposed high-resolution CNN method to segment skin lesion. Firstly, input is taken as high-resolution feature maps for extracting spatial details around the boundary. Thereafter, spatial and channel-wise dimensions are utilized for detecting accurate lesion boundary. Pour et al. [34] incorporated image representations of the transform domain to the CNN, which resulted in the higher Jaccard index and less training time. They used the CIELAB colour space of the image dataset and also flipped all the images in order to increase the dataset size. In post-processing, image processing operations have been used to segment the lesion.

The work on classification of skin lesions into different categories have also been done by many researchers. The works are based on direct classification of lesions or after segmenting the lesions. The classification of melanoma using ensemble method of neural network has been done by Xie et al. [46] where they have worked on the dermatology images collected from the hospital and showed promising results on their dataset. Satheesha et al. [39] on the other hand worked on the standard datasets (ATLAS, PH2, ISIC) for melanoma classification. They find 3-D reconstruction, depth and 3-D shape based features for the classification. Menegola et al. [28] used transfer learning techniques of deep learning to classify skin images into (1) benign and malignant, (2) benign, malignant and carcinoma. Mahbod et al. [24] proposed a fully automatic classification system where they fine-tuned CNNs on skin images which are then used to train various support vector machine (SVM) classifiers in order to get final prediction. Thus, they call their method as ensemble method. Ghalejoogh et al. [15] also worked on ensemble classification methods where they have classified skin lesion images as melanoma, dysplastic and benign. They have introduced hybrid structure based on stacking (SBS) and hierarchical SBS (HSBS) technique to combine the heterogeneous classifiers and performed five fold cross-validation procedure. Sadri et al. [38] proposed a fixed grid wavelet network (FGWN) for predicting malignant melanoma from their own collected dataset. The work on the same problem done by Akram et al. [5] where they have used the saliency estimation approach for better results. The biggest disadvantage of their method was that they have not used test dataset provided by ISBI 2016 for testing purpose. However, dividing the whole dataset consisting of training and testing images into 50:50; and proving that they have achieved the classification accuracy of 99.2%, and thus accuracy cannot be considered for the standard dataset as the testing dataset is already available and therefore results should also be shown on that dataset as well for comparison.

Premaladha and Ravichandran [35] proposed an efficient algorithm to identify and classify melanoma. Initially, they performed image enhancement using contrast limited adaptive histogram equalization technique (CLAHE) and median filter. Thereafter, normalized Otsu's segmentation (NOS) is used to segment the lesion. Further, 15 features have been extracted

which are then given as input to deep learning based neural networks and hybrid adaboost-SVM algorithms. Schaefer et al. [40] perform lesion segmentation at the first stage, which is then used for extracting colour, texture and shape based features. Thereafter, those features are used by the ensemble learning approach for classification where each classifier is trained individually on features and each time removes predictors which are not required. Then neural network is combined with remaining classifiers to get the final result. Al-masni et al. [7] has also worked on both skin lesion segmentation and their classification. The method which they have utilized was based on integrated deep convolutional networks and identified the boundary of lesions by using FrCN [6]. Further, a CNNs classifier was applied on the segmented skin lesions for classification. Xie et al. [48] have worked for mutual bootstrapping deep CNN (MB-DCNN) model. However, the limitation of their methods is that it has to reduce the image size which is even less than the half of image size due to which relevant information cannot be extracted. The requirement of accurate diagnosis of skin cancer is increasing because cases are increasing everyday and thus needs more research focus for developing a better CAD system that will help medical doctors in timely treatment. Mahbod et al. [25] have identified the impact of skin lesion segmentation on its classification. They have used either manually or automatically created segmentation masks in both training and test phases in different scenarios and investigated the classification performances on EfficientNet [42]. Kadampur and Riyaee [21] have proposed a deep learning based method which is based on setting different parameters for deep layers of the network. In their own study, they have said that "There is no rule of thumb for setting these parameters." which is not theoretically possible and thus can be considered as its drawback. On the other hand, the recent study done by Tyagi and Mehra [44] proposed the CNN based method for skin lesion classification; however, in their study, they are mentioning that "This study uses a dataset of 1000 dermoscopy skin lesion images of 545 BCCs and 455 non-BCCs or benign images as the input sets. This dataset is taken from ISBI-2016 Dataset and available on: www.isic-archive.com." which cannot be true as dataset contains only benign and malignant cases have not disclosed their subcategories, and number of total images in the dataset is 900 for training and 379 for testing. Thus, the results obtained in the paper are baseless.

Now, the works which are related to feature extraction methods are discussed here. Several feature extraction methods have been developed so far in the field of computer vision and image processing which have shown their importance especially in medical image processing. The most commonly used feature descriptor till now is a local binary pattern (LBP) which was proposed by Ojala et al. [31]. After that many of its variants have come like rotation invariant LBP (LBP^{ri}), uniform LBP (LBP^{u2}) and rotation invariant uniform LBP (LBP^{riu2}), and all have shown their effectiveness [32]. LBP utilized neighbouring information by binarizing the neighbours in 0 and 1 form in order to generate features. Thereafter, so many methods have come like local ternary patterns (LTP) proposed by Tan and Triggs [43]. It is a three value code by having one more code value for neighbours, that is -1 including 0 and 1 not like LBP which has 2 value code (0 and 1). Completed local binary pattern (CLBP) proposed by Guo et al. [16] was based on extracting information from the magnitude vectors and the centre pixels. Dubey et al. [11] proposed a local wavelet pattern (LWP) for characterizing CT images where they used wavelet decomposition for identifying the relationship between neighbouring pixels. In their other work [10], they have proposed a local diagonal extrema pattern (LDEP) which is based on first-order local diagonal derivatives for feature extraction. Local directional relation pattern (LDRP) was proposed by Dubey et al. [12] where for extracting features they utilized the connection among the centre pixel and the encoded directional neighbours. Local gradient of gradient pattern (LG2P) descriptor was proposed by Gautam et al. [13] where gradients of neighbours were computed twice for identifying the relationship between neighbouring pixels and centre pixel of the brain CT scan image. Song et al. [41] worked on the classification of textures for which they have proposed a spatially weighted order binary pattern (SWOBP) by introducing a colour gradient channel and exploring a multi-channel colour order pattern for finding features from images. Local multiple patterns (LMP) feature descriptor proposed by Wankou et al. [49] for identifying the ration of change of stimulus to the stimulus itself which play very important role in human perception and their method was based on Weber's law. Shamaileh et al. [30] have proposed a new rotation invariant texture descriptor (Feat-WCLTP) for texture classification. Their method was based on RDWT transform which is a robust wavelet transform with the combination of completed local ternary pattern (CLTP) descriptor [36], which was again the combination of CLBP [16] and LTP [43]. However, Feat-WCLTP lacks a practical approach as they have used a combination of methods proposed by other authors.

3 | BACKGROUND PRELIMINARY

In this section, we have discussed the technical background of feature extraction methods.

3.1 | Local binary pattern

Local binary pattern (LBP) [31] was designed to extract information from the local neighbourhood of grayscale image. LBP later has indicated amazing performance in various applications in terms of discriminative performance and computational complexity [32]. Originally, it used 3×3 neighbourhood to assign a label to its neighbour pixels by thresholding them with the centre pixel value to form a binary number.

Its working can be understood with the help of Figure 2 and equations given below (Equations 1 and 2).

$$LBP_T = \sum_{t=1}^{T} 2^{(t-1)} \times f_1(g_t - g_c) \tag{1}$$

$$f_1(m) = \begin{cases} 1, & m \geq 0 \\ 0, & else \end{cases}, \tag{2}$$

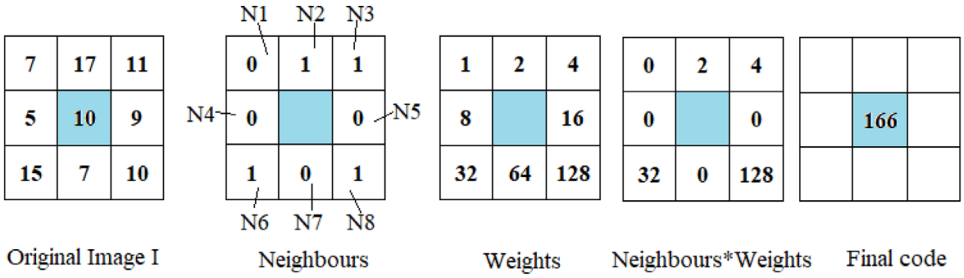

FIGURE 2 Calculation of LBP code

where g_c represents gray-value of centre pixel, gray-value of neighbour is g_t, T is the number of neighbours around g_c. LBP pattern calculation is depicted in Figure 2. After standard LBP many of its variants came into existence like uniform, rotation invariant and rotation invariant uniform LBP.

In uniform local binary pattern (LBP^{u2}) uniform appearance of binary code with a maximum transition of 2 that is 1 to 0 and 0 to 1 is computed. Due to this it reduces the feature vector length and improves the performance of the classifiers. In LBP, u is given as:

$$u(LBP_T) = \left|f(g_{T-1} - g_c) - f(g_0 - g_c)\right| + \sum_{t=1}^{T-1} \left|f(g_t - g_c) - f(g_{t-1} - g_c).\right| \quad (3)$$

The mapping from standard LBP to LBP^{u2} has $P \times (T-1) + 3$ output values that corresponds to 2^T various binary patterns.

Rotation invariant LBP (LBP^{ri}) is the other variant which results in the same output value even if gray-values of the images are rotated by a certain degree. Hence, removes the drawback of LBP. LBP^{ri} is given as:

$$LBP_T^{ri} = min\{ROR(LBP_T, r) \mid r = 0, 1, \ldots, T-1\}, \quad (4)$$

where $ROR(q, r)$ performs circular bit-wise right shift on the P-bit number q r times and rotation invariant uniform LBP (LBP^{riu2}) could be defined as

$$LBP_T^{riu2} = \begin{cases} \sum_{a=0}^{T-1} d(g_a - g_c), & \text{if } U(LBP_T) \le 2. \\ T+1, & \text{else} \end{cases} \quad (5)$$

Example 1 shows the complete detail for the calculation of LBP codes.

Example 1. Finding the neighbours of centre pixel from an image I and calculation of LBP code.

As per Ojala et al. [31], if we have to find the LBP code of 3×3 image I as given in Figure 2. Then, all the neighbours (N1, N2,…..,N8) of the centre pixel (indicated in blue colour) are compared with it which is 10 here. Finally, each neighbour is multiplied by the weights assigned to them, please refer to Figure 2 for more details. Likewise, if we have images of bigger size than accordingly LBP codes will be calculated.

3.2 | Local ternary patterns

After the popularity of LBP and its variant, Tan and Triggs [43] proposed local ternary patterns (LTP). As per the paper, LBP has the drawback that it does not extract required features if the image is sensitive to noise in local neighbourhoods. LTP had tried to overcome this limitation up to some extent. Their method was extended to three-values code (0, 1 and −1) instead of two-values code (i.e. 0 and 1 in LBP). This means that if gray values in a zone of width $\pm w$ around g_c then they are mapped to zeros, which are above this are mapped to +1 and which are below it to -1, and this is represented by:

$$f(g_i, g_c, w)' = \begin{cases} 1 & g_i \ge g_c + w, \\ 0 & |g_i - g_c| < w \\ -1 & g_i \le g_c - w. \end{cases} \quad (6)$$

Finally, lower and upper LTP codes are calculated where LTP upper consider only those neighbours whose values are mapped as positive and map all other neighbours to 0. In LTP lower, only those neighbours are considered whose mapped values are -1 and all other remaining neighbours values are mapped to 0. Figure 3 depicts the calculation of LTP feature code. The binary codes which are represented in figure are further converted to decimal codes. For our experiments, we have chosen w as 5, which was also chosen by [43] and for more details readers are referred to that paper.

For all other feature descriptors which we have used for comparison such as LWP, LDEP and LDRP, their complete details can be found in [10–12].

4 | PROPOSED METHODOLOGY

In this section, we have discussed the proposed methodology for the classification of skin lesions from dermoscopic images. This section is divided into two parts: feature extraction (in Section 4.1) and classification (in Section 4.2), which are discussed below in detail.

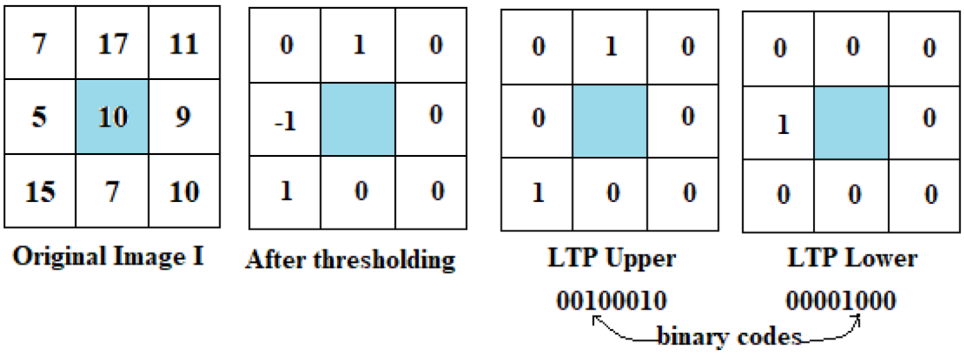

FIGURE 3 Calculation of LTP code

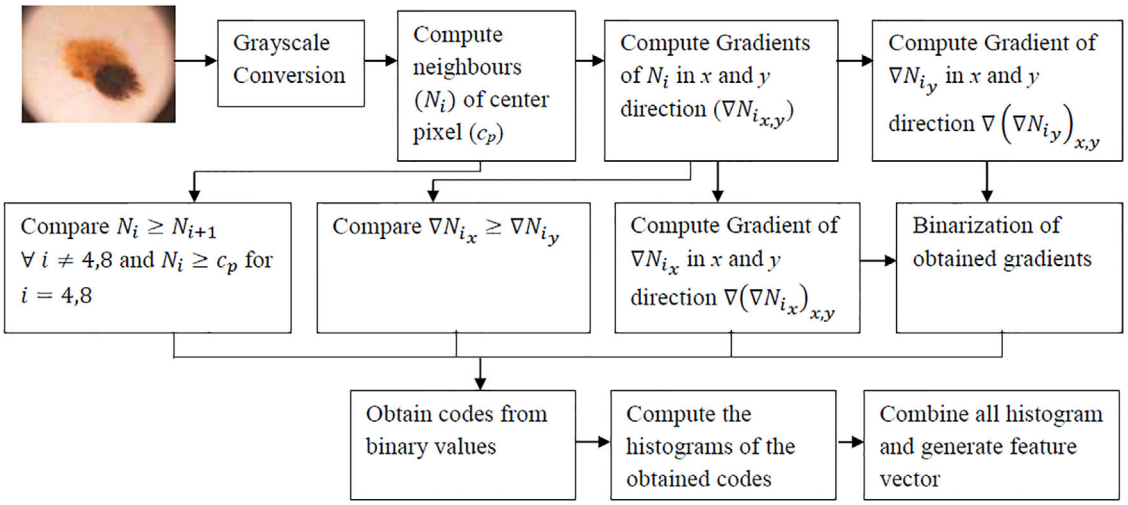

FIGURE 4 Workflow of proposed feature descriptor

4.1 | Feature extraction

In this section, the proposed feature extraction method is discussed in detail where we find those features which will help in accurate classification of images. Figure 4 depicts the complete procedure to compute the feature vector and complete details are given below.

In the first step of our method, we will find all neighbours of the centre pixels in eight different directions. Suppose, we have an image size of 3×3 then in that case different neighbours of the centre pixel are at left, right, top, bottom, left-top, right-top, bottom-left and bottom-right directions. However, for our method to work, image size should be at least 5×5. In order to understand what are different neighbours of 5×5 image, please refer to Figure 5. In the figure, we have image I where the number of pixels which are part of centre depends on the size of the image which means if we have image of size $N \times N$ then we will have $N-2 \times N-2$ pixels for the centre as well as for neighbours. To better understand this, the pixels which are part of centre pixels have intensities of 100, 30, 56, 67, 25, 100, 56, 20 and 80. Now, eight different neighbours of these centre pixels are indicated in different directions of the image I in Figure 5.

After finding all eight neighbours, our next step is to compute the gradient of all the neighbours in x and y directions ($\nabla N_{i_{x,y}}$). In our work, we have used a gradient() method of MATLAB R2019b, where it calculates values of corner points in x and y direction by obtaining the difference between the adjacent neighbour and the point. However, for interior points, gradient is obtained by the difference of neighbour in the positive direction of the x-axis and in the negative direction of x-axis (likewise for y-direction), which is then multiplied by 0.5. Figure 6 shows gradient values obtained in x and y directions of image I. The main aim of computing the gradient is to identify the direction of intensity change of neighbouring pixels. So after computing gradients in both the directions of all the eight neighbours according to Equation (7), then we compare the values obtained in x direction with those in the y direction for identifying the difference in both directions (Equation (8)). For extracting features based on the neighbours of neighbours, we have used Equation 9, in which each neighbour is compared with its adjacent neighbour, unlike LBP which compare neighbours with only centre pixel. Further, gradient of Equation (7) is computed again in both the direction as given in the Equation (10) and Equation (11). This computation of gradients helps in finding the exact changes in the direction of texture pattern. In the

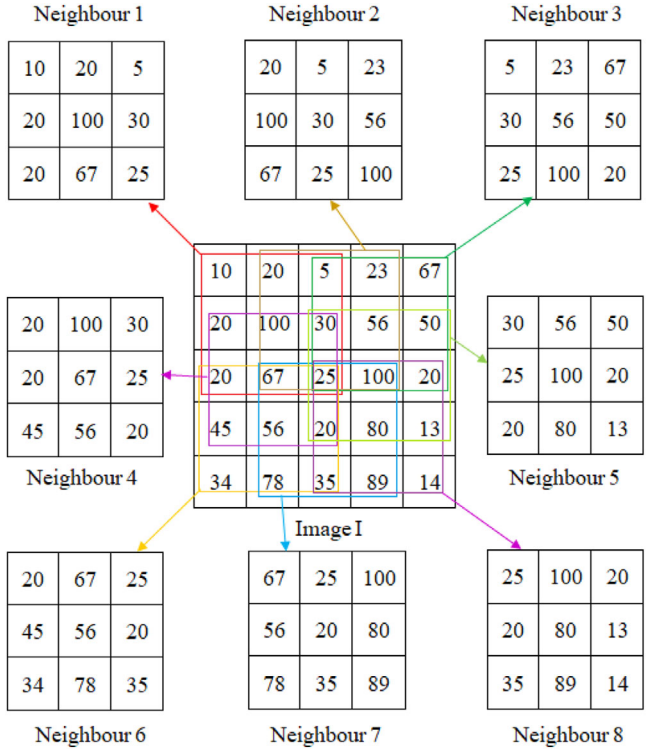

FIGURE 5 Eight Neighbours of Image I of size 5×5

next step, all the obtained values from Equation (10) and Equation (11) are binarized that is values which are greater than 0 will be assigned the value of 1 otherwise 0, please refer Equation (12).

$$\nabla N_{i_{x,y}} = \sum_{i=1}^{P} \begin{bmatrix} \frac{\partial N_i}{\partial x} \\ \frac{\partial N_i}{\partial y} \end{bmatrix} \qquad i = 1, 2, 3, \ldots .., 8 \tag{7}$$

here P means the total number of neighbours of the centre pixels (cp), here it is 8 and N_i represents the ith neighbour.

$$C_i = \begin{cases} 1, & \nabla N_{i_x} \geq \nabla N_{i_y} \\ 0, & \text{else} \end{cases} \tag{8}$$

$$V_i = \begin{cases} 1, & N_i \geq N_{i+1} \forall i \neq 4, 8 \quad \& \\ & N_i \geq c_p \text{ for } i = 4, 8 \\ 0, & \text{else} \end{cases} \tag{9}$$

$$\nabla(\nabla N_{i_x})_{x,y} = \sum_{i=1}^{P} \begin{bmatrix} \frac{\partial \nabla N_{i_x}}{\partial x} \\ \frac{\partial \nabla N_{i_x}}{\partial y} \end{bmatrix} \tag{10}$$

$$\nabla(\nabla N_{i_y})_{x,y} = \sum_{i=1}^{P} \begin{bmatrix} \frac{\partial \nabla N_{i_y}}{\partial x} \\ \frac{\partial \nabla N_{i_y}}{\partial y} \end{bmatrix} \tag{11}$$

$$[\lambda_{\nabla(\nabla N_{i_x})_{x,y}}, \lambda_{\nabla(\nabla N_{i_y})_{x,y}}] = \begin{cases} 1, & \nabla(\nabla N_{i_{x,y}})_{x,y} \geq 0 \\ 0, & \text{else} \end{cases} \tag{12}$$

where λ represents binarized value and we named it as $\lambda_{\nabla(\nabla N_{i_x})_{x,y}} = \lambda_{i_{G1}}$ and $\lambda_{\nabla(\nabla N_{i_y})_{x,y}} = \lambda_{i_{G2}}$.

Further, after computing the binarized value of all the eight neighbours from Equation (8), (9), (10) and Equation (11), the next step is to generate the pattern code from them using Equation (13).

$$ReIP_i = \sum_{i=1}^{P} 2^{(i-1)} \times (\lambda_{i_{G1}}, \lambda_{i_{G2}}, C_i, V_i) \tag{13}$$

where $ReIP_i$ represents our proposed Regional Information Pattern (ReIP) codes. After calculating codes from the above four equations generate the 1-D histogram which computes 256 features for each of $\lambda_{i_{G1}}, \lambda_{i_{G2}}, C_i$ and V_i, and finally combine those features to obtain feature one feature vector of length 1536.

Example is given below to better understand the proposed methodology.

Example 2. Computation of Pattern Codes:

- First, identify all the neighbours of the centre pixels of the image as depicted in Figure 5.
- Then for all neighbours gradient is computed in both x and y direction according to Figure 4, also can be seen in Figure 7.
- Binarize the gradient values of neighbours and placed them from right to left in such a way that neighbour N1 value should be placed at the first place and then N2 and then so on till N8 is at the left most position. For example: Let's say instead of using neighbour, we use N, then the neighbour's sequence would be N8N7N6N5N4N3N2N1 and according to the binary values placed in the yellow box then the sequence obtained will be 01000110.
- Further, the obtained sequence is used to calculate the code by converting this eight digit binary number to decimal. For example:$0 * 2^7 + 1 * 2^6 + 0 * 2^5 + 0 * 2^4 + 0 * 2^3 + 1 * 2^2 + 1 * 2^1 + 0 * 2^0 = 70$ which means 70 is the code value obtained for one of the centre pixel values which is at the top-left most location. Likewise, we can calculate the code for pixels as well.

After obtaining the codes for all the pixels of the centre pixels, we get the new image of size $(N-2) \times (N-2)$ if original image is of size $N \times N$. For example, in Figure 5, we have image of size 5×5 and in Figure 7(c) we obtained the codes of size 3×3. Likewise, according to the work flow diagram of proposed methodology which is depicted in Figure 4 we obtained codes of six different types using Equation (13). Thereafter, our next step is to generate the 1-D feature vector by computing the histograms of obtained codes. The generated histograms will then be combined and will work as the new feature descriptor for the classification of images.

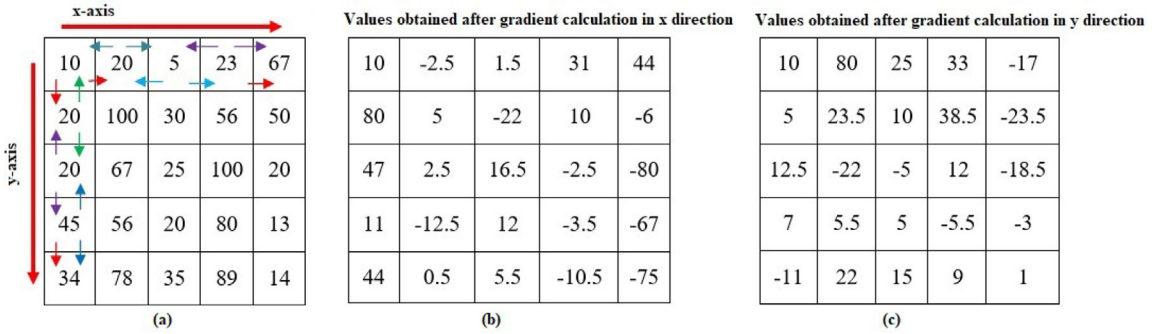

FIGURE 6 (a) Input image I, gradient of image in (b) x direction and (c) y direction

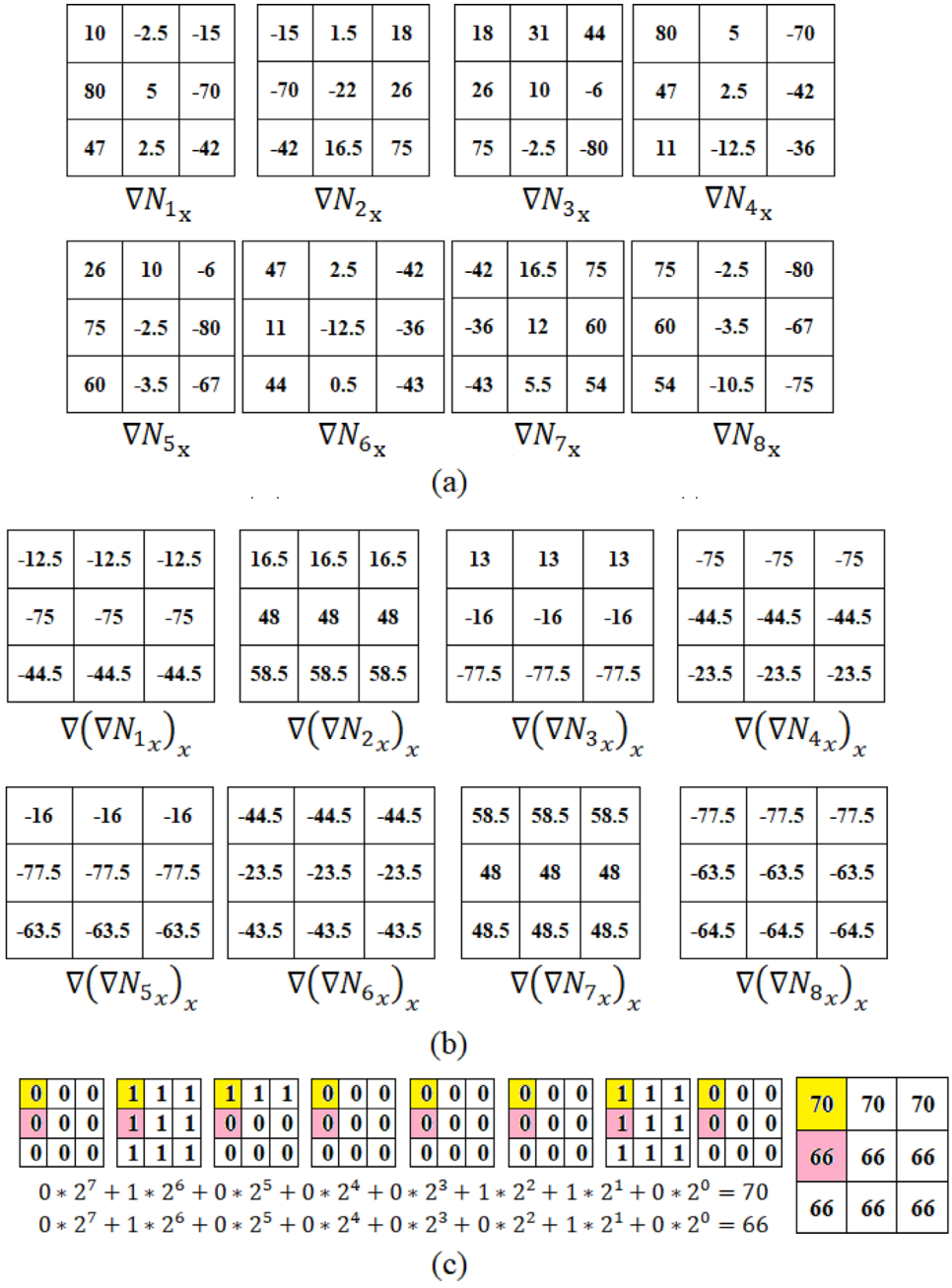

FIGURE 7 (a) Computation of gradients in x direction of all the neighbours of centre pixel in Figure 5, (b) gradient is again computed for neighbours in (a) in x direction and (c) peforming binarization of all the values in (b) for obtaining the codes of all the neighbours

ALGORITHM 1 Classification of features extracted from the images using cross-validation

Input : Features of Training Image dataset (F)
Output: Classification Accuracy
function classify (F);
Divide the feature set into k equal sets S
Classification using the linear SVM, and medium kNN, ensemble bagged trees and ensemble boosted trees.
for $i = 1$ *to* k **do**
    choose the classifier C_n for classification task (n is number of classifiers)
        TestingSet=S_i and
        TrainingSet=all S except S_i
        train classifier on TrainingSet and perform testing on TestingSet
        Predict the accuracy of the classifier.
end
Prediction of average classification accuracy.

4.2 | Classification

In this section, we will focus on the classification of images by utilizing the useful features. For the classification of skin cancer from dermoscopic images provided by ISIC Archive 2016, we have focused on different classification techniques such as (1) 10 fold cross-validation on the training dataset, (2) classification of testing dataset provided the model should be trained on training dataset (3) holdout validation where 70% of training data is used for training and 30% of it is used for testing.

The algorithm of k-fold cross-validation method is given below:

For the second classification method, we will train the classifier using features extracted from the training dataset which is provided by ISIC 2016. Further, test dataset in ISIC 2016 is used for testing which follows the same procedure of feature extraction as discussed in Section 3.1. Finally, the classification accuracy is determined to check whether our method is suitable for medical practice or not. Likewise, for a 3rd classification method which is holdout validation we randomly split the training dataset of ISIC 2016 into 7:3 ratio of training and testing set. The final accuracy of the classification model is observed on the testing dataset. The classifiers which we have chosen to check the efficacy of our proposed feature extraction method are linear SVM, medium k Nearest Neighbour (kNN), ensemble bagged trees and ensemble boosted trees. The experiments which have been carried out on these classifiers with our feature descriptor are given in the next section.

5 | EXPERIMENTAL RESULTS

This paper has focused on the classification of skin cancer lesion as benign and malignant. The dataset which we have used for carrying out experiments have been made freely available which has a title of "ISIC 2016: Skin Lesion Analysis Towards Melanoma Detection" [17]. ISIC is the International Skin Imaging Collaboration (https://isic-archive.com/) which is supported by the International Society for Digital Imaging of the Skin (ISDIS). The ISIC 2016 consists of ISBI2016_ISIC_Part3_Training_Data and ISBI2016_ISIC_Part3_Test_Data datasets with their ground truth information in *.csv* format. In both datasets, dermatology images of benign and malignant skin cancer is present. The number of cases in both the datasets is mentioned in the Table 1 and we have used both the datasets for experiments where all dermatology images are coloured images of different sizes which varies from 722×542 to 4288×2848.

TABLE 1 Melanoma cases distribution into two categories

Dataset	Type of melanoma	Number of cases
ISBI2016_ISIC_Part3_Training_Data	Benign	727
	Malignant	173
ISBI2016_ISIC_Part3_Test_Data	Benign	290
	Malignant	89

TABLE 2 Feature vector length of various methods and elapsed time to extract features from image of size $1536 \times 2048 \times 3$

Feature descriptor	Length	Elapsed time (s)
LBP	256	0.22
LBP^{u2}	59	1.13
LBP^{ri}	36	1.02
LBP^{riu2}	10	0.98
LTP	512	1.51
LWP	256	1.40
LDEP	24	1.28
LDRP	1024	0.16
ReIP	1536	4.31

For checking the efficacy of proposed descriptor we have conducted four experiments using different classifiers like experiment 1 by using linear SVM, experiment 2 by medium kNN (here k is 10), experiment 3 by ensemble bagged trees and experiment 4 by using ensemble boosted trees on Intel(R) Core i5-6200U CPU @ 2.30 GHz processor with 8 GB RAM. The first step before classification which we have followed is based on feature extraction. Feature extraction codes of LBP, its variants, LTP, LWP, LDRP and ReIP methods in 2-D form are depicted in Figure 8; however, for LDEP, 2-D codes have not been identified. All 2-D images of obtained codes are further transformed to 1-D feature vector for classification task. If more than one feature code images are there for a descriptor then their 1-D forms are concatenated to form a single feature vector. Table 2 depicts the feature vector length and elapsed time (in seconds) of the various descriptors described above. Elapsed time is computed on a $2048 \times 1536 \times 3$ size image taken from the ISIC 2016 training dataset. In all four experiments, we have performed classification using 10-fold cross-validation (we call it as method 1 i.e. M1), classification of ISBI2016_ISIC_Part3_Test_Data dataset by training

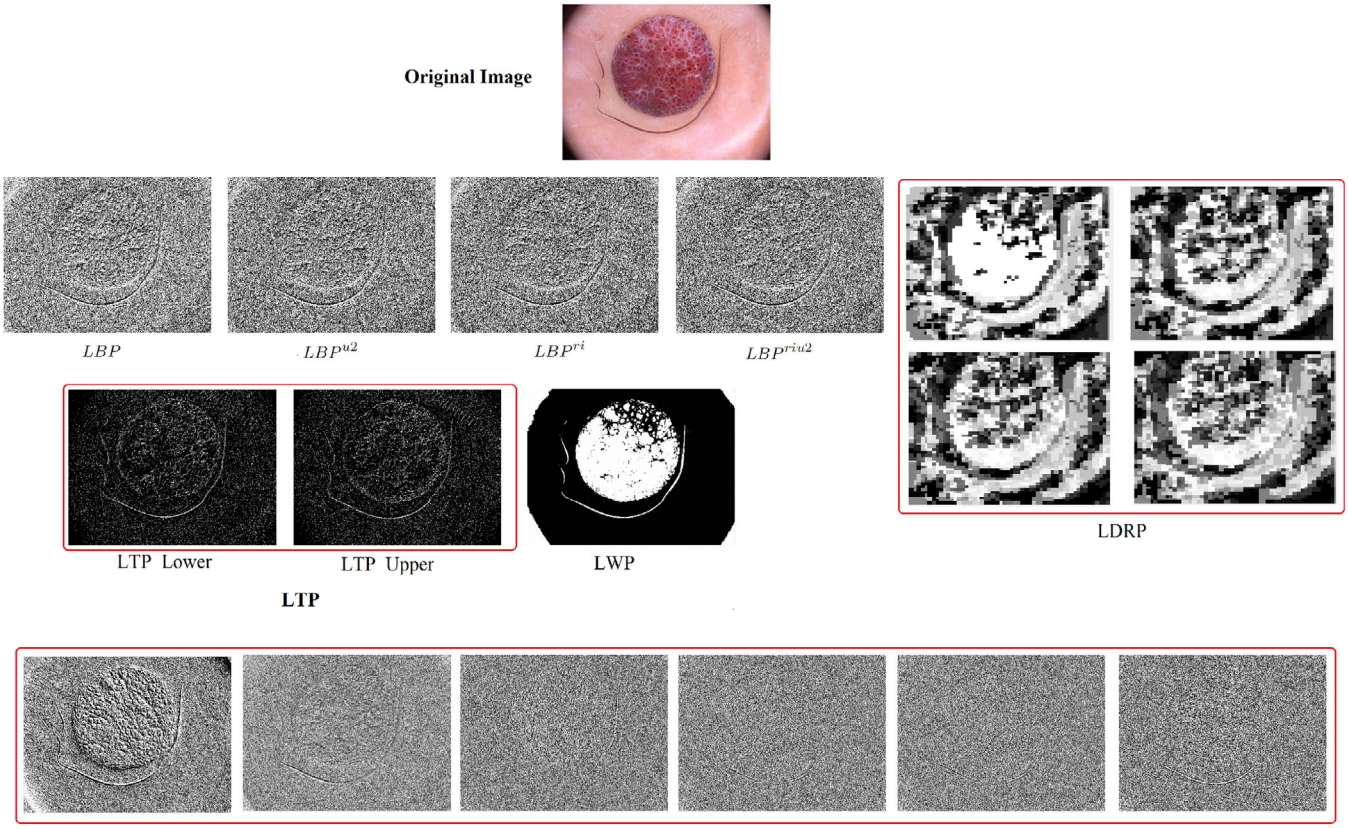

FIGURE 8 2-D representation of features extracted by different feature extraction methods from input image

ISBI2016_ISIC_Part3_Training_Data dataset (M2) and hold-out validation of training dataset (M3). The results of the experiments are given in terms of accuracy, TPR and FPR [13]; here receiver operating characteristics (ROC) curves are used to show the values obtained by TPR and FPR.

5.1 | Experiment 1 using Linear SVM

In this section, we have classified the datasets given in Table 1 using linear SVM. Firstly, we performed classification using 10 fold cross-validation on the training dataset where the final accuracy is the average of all the accuracies obtained in testing different fold of the dataset. The results obtained in this experiment show that almost all the feature descriptors are giving the same accuracy with a variation of less than 2% and this can be seen clearly in Table 3 and ROC curve in Figure 9(a). The results of experiments using method 2 (M2) are given in the second column of Table 3 and ROC curves in Figure 10(a). The results obtained by feature descriptors using method 3 (M3) are given in column 3 and in Figure 11(a). With linear SVM, M2 gives the highest classification accuracy of 83.64% on a testing dataset with a huge difference with other feature descriptors. In case of M3, linear SVM achieved an accuracy of 82.59 % with ReIP descriptor and is highest among others. All the three classification techniques proved that our method is able to give more accurate result when used with linear SVM as compared to others.

TABLE 3 Accuracy (in %) obtained by different feature descriptors using linear SVM

Classifier	Accuracy (M1)	Accuracy (M2)	Accuracy (M3)
LBP	81.22	77.57	79.26
LBP^{u2}	80.78	76.52	80.74
LBP^{ri}	81.23	77.57	81.48
LBP^{riu2}	80.78	76.52	80.74
LTP	80.56	76.78	81.11
LWP	80.67	76.52	79.63
LDEP	80.78	76.52	80.74
LDRP	81.22	75.99	80.74
ReIP	81.78	83.64	82.59

5.2 | Experiment 2 using Medium *k*NN

In this section, we have performed experiments using medium *k*NN as a classifier. Here also classifications have been performed by using three different methods that is M1, M2 and M3 as mentioned in the above sections. In all experiments using these three methods we have found that proposed descriptor gave better classifications than others as depicted in Table 4. In case of M1, ReIP achieved an accuracy of 81.33% whereas LBP^{u2} and LDRP have achieved 79.67% accuracy and this can also be seen in Figure 9(b). In method 2, LBP, LTP and ReIP

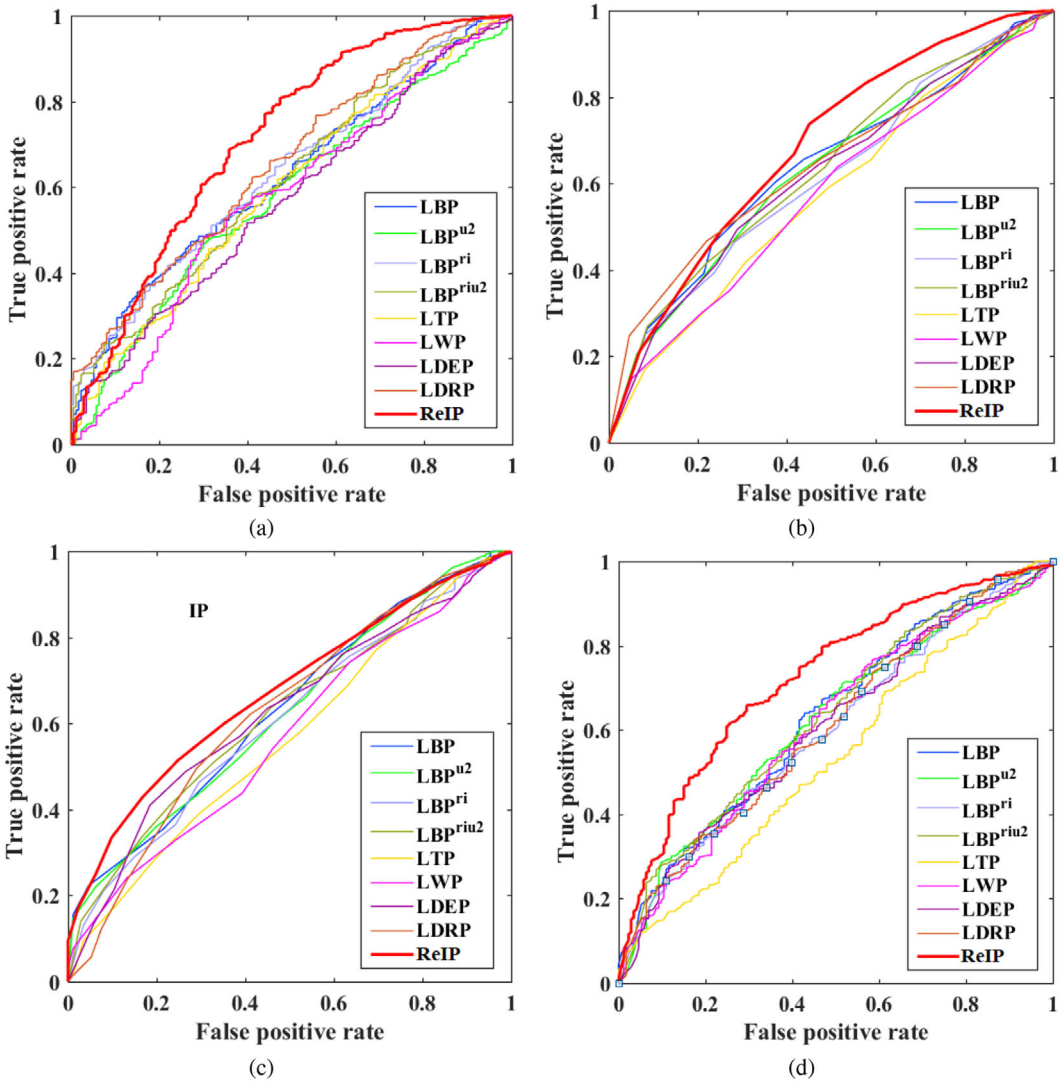

FIGURE 9 ROC curves of 10-fold cross-validation results using (a) linear SVM, (b) medium *k*NN, (c) ensemble bagged trees and (d) ensemble boosted trees

TABLE 4 Accuracy (in%) obtained by different feature vectors using medium *k*NN

Classifier	Accuracy (M1)	Accuracy (M2)	Accuracy (M3)
LBP	80.11	77.31	80.37
LBP^{u2}	79.67	76.25	81.11
LBP^{ri}	80	76.52	80.37
LBP^{riu2}	79.78	75.73	80.74
LTP	80.22	77.04	79.63
LWP	80.33	75.46	80.74
LDEP	80.11	76.78	80.74
LDRP	79.67	75.99	81.11
ReIP	81.33	77.57	81.48

have achieved an accuracy of approximately 77% when testing is performed using ISBI2016_ISIC_Part3_Test_Data dataset; however, ReIP performs best with 77.57% accuracy. If we perform classification by method 3 using *k*NN classifier then in that case also ReIP is able to extract more relevant feature from the images and thus performs better classification as compared to others. ROC curves obtained by all the feature descriptors using M2 and M3 are depicted in Figures 10(b) and 11(b), respectively.

5.3 | Experiment 3 using ensemble bagged trees

This section contains information about skin cancer classification using ensemble bagged trees. All the classification results obtained using M1, M2 and M3 are depicted in Table 5 and have also shown results using true positive rate and false positive rate in Figures 9(c), 10(c) and 11(c) with the help of ROC curves. The accuracy obtained by M1 using ReIP is 80.89 % which is higher than others while performing cross-validation of the training image dataset. The accuracy obtained by our

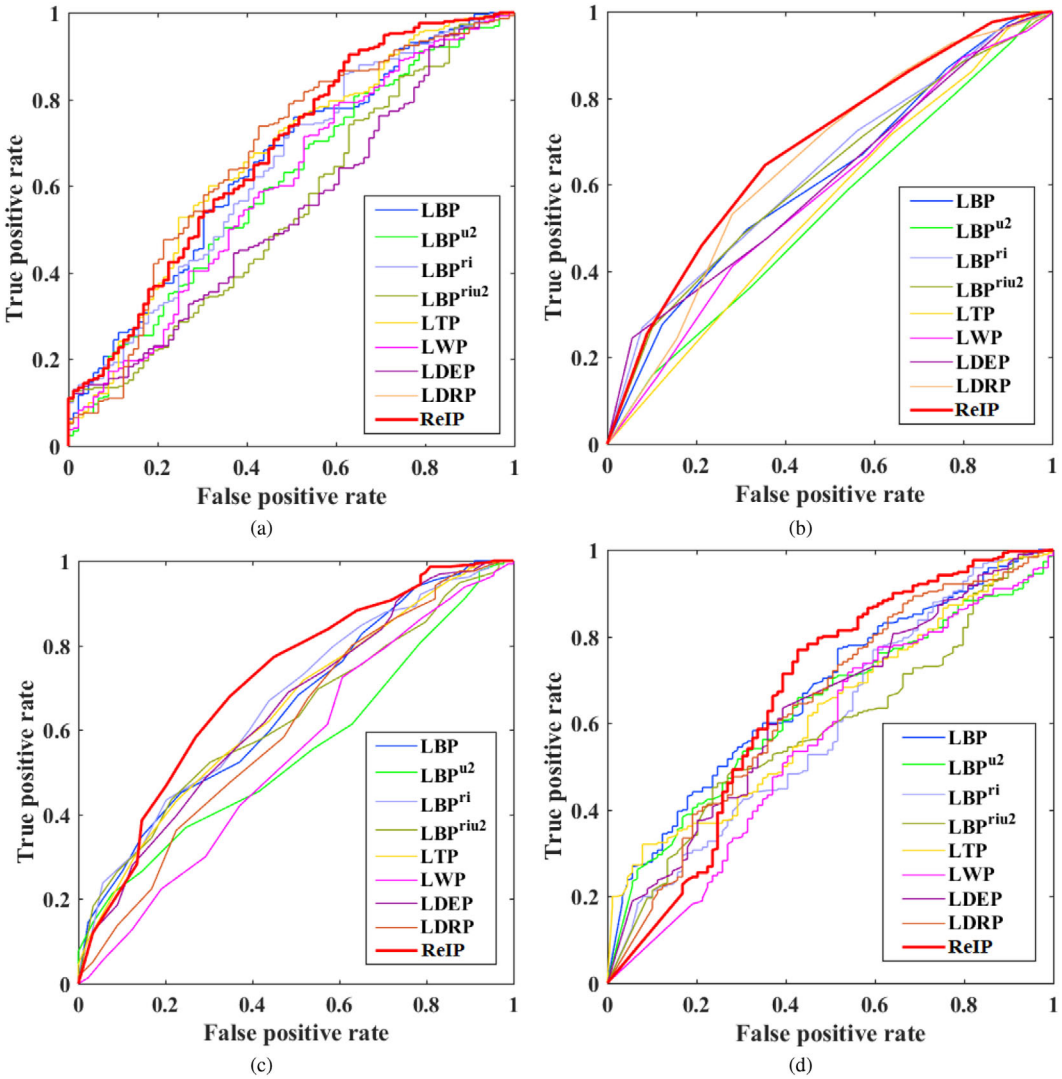

FIGURE 10 ROC curves obtained by (a) linear SVM, (b) medium *k*NN, (c) ensemble bagged trees and (d) ensemble boosted trees using the second classification method

TABLE 5 Accuracy (in %) obtained by different feature vectors using ensemble bagged trees

Classifier	Accuracy (M1)	Accuracy (M2)	Accuracy (M3)
LBP	79.67	78.10	78.89
LBP^{u2}	79.56	76.78	78.89
LBP^{ri}	78.78	75.99	78.15
LBP^{riu2}	78.78	75.46	78.89
LTP	80.44	77.57	81.48
LWP	80.11	75.46	80
LDEP	77.78	78.10	77.41
LDRP	80.46	77.04	81.11
ReIP	80.89	79.95	82.12

ReIP using M2 is 79.95 % and in case of M3 also the accuracy obtained is 82.12 % and this shows that our feature descriptor gives higher accuracy than all others. Hence, we can say that ReIP performs better even when images are classified with ensemble bagged trees.

5.4 | Experiment 4 using ensemble boosted trees

Ensemble boosted trees classifier has been used in this section for experimenting with feature descriptors using the three classification methods which we have discussed earlier. From all the experiments, it has been found that proposed feature descriptor ReIP is able to classify images of lesions more easily as compared to other descriptors and details are given in the Table 6. In M1, ReIP obtained an accuracy of 81%, while in M2, the accuracy achieved is 78.36%, which is very high as compared to others and if we classify images using M3 then in that case as well ReIP achieved the highest classification accuracy with ensemble

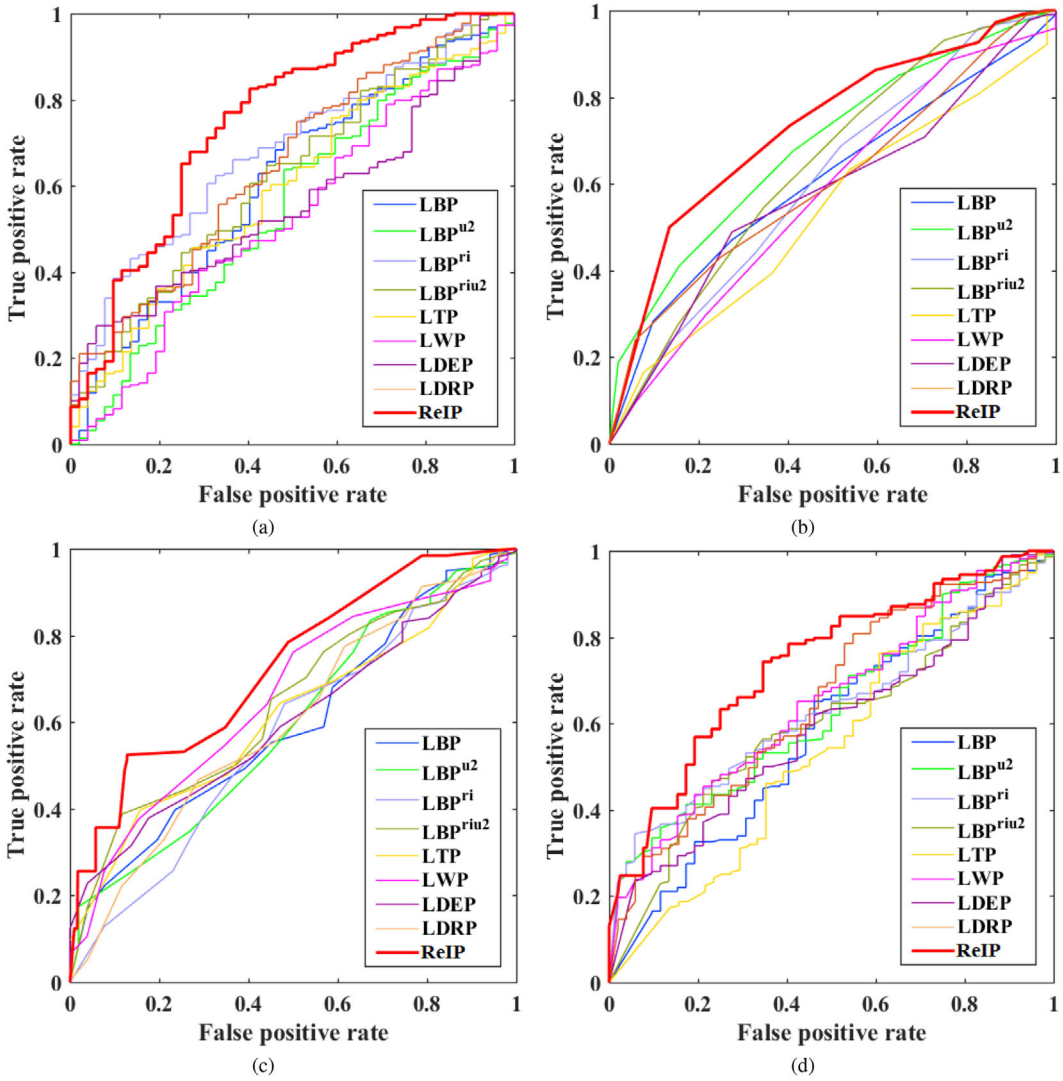

FIGURE 11 ROC curves obtained by (a) linear SVM, (b) cubic SVM, (c) ensemble bagged trees and (d) ensemble boosted trees using the third classification method

TABLE 6 Accuracy (in %) obtained by different feature vectors using ensemble boosted trees

Classifier	Accuracy (M1)	Accuracy (M2)	Accuracy (M3)
LBP	79.78	77.04	78.15
LB^{u2}	79.56	74.67	80.37
LBP^{ri}	79.89	76.78	79.26
LBP^{riu2}	79.78	76.78	79.26
LTP	79.45	76.52	80.74
LWP	79.11	74.14	80.74
LDEP	79.44	77.31	81.48
LDRP	80	75.20	79.26
ReIP	81	78.36	82.78

boosted trees classifier. The results are also shown with the help of ROC curves in Figures 5(d), 6(d) and 7(d) where red curve is for ReIP. Hence, we can say that in case of ensemble boosted trees classifier as well our feature extraction method is giving better classification results.

6 | DISCUSSION

The discussion of the results obtained by different machine learning algorithms with various feature descriptors along with our proposed one is discussed here.

The classification results which we have obtained by M1 where cross-validation technique has been used show that linear SVM gives the highest classification accuracy by using the proposed ReIP descriptor as compared to other classifiers. After linear SVM results, medium kNN where the value of k taken is 10 gives better results and after that ensemble boosted trees and ensemble bagged trees performed better.

In case of M2, which uses different datasets for training and testing as given in Section 4 shows that ReIP performs better than other descriptors. Further, when we compare

TABLE 7 Comparative analysis of all classifiers with various feature descriptors on testing dataset

Feature descriptor	Classification method	Accuracy (%) (Linear SVM)	Accuracy (%) (*k*NN)	Accuracy (%) (ensemble bagged trees)	Accuracy (%) (Ensemble boosted trees)
LBP [31]	M1	81.22	80.11	79.67	79.78
	M2	77.57	77.31	78.10	77.04
	M3	79.26	80.37	78.89	78.15
LBP^{u2} [32]	M1	80.78	79.67	79.56	79.56
	M2	76.52	76.25	76.78	74.67
	M3	80.74	81.11	78.89	80.37
LBP^{ri} [32]	M1	81.23	80	78.78	79.89
	M2	77.57	76.52	75.99	76.78
	M3	81.48	80.37	78.15	79.26
LBP^{riu2} [32]	M1	80.78	79.78	78.78	79.78
	M2	76.52	75.73	75.46	76.78
	M3	80.74	80.74	78.89	79.26
LTP [43]	M1	80.56	80.22	80.44	79.45
	M2	76.78	77.04	77.57	76.52
	M3	81.11	79.63	81.48	80.74
LWP [11]	M1	80.67	80.33	80.11	79.11
	M2	76.52	75.46	75.46	74.14
	M3	79.63	80.74	80	80.74
LDEP [10]	M1	80.78	80.11	77.78	79.44
	M2	76.52	76.78	78.10	77.31
	M3	80.74	80.74	77.41	81.48
LDRP [12]	M1	81.22	79.67	80.46	80
	M2	75.99	75.99	77.04	75.20
	M3	80.74	81.11	81.11	79.26
ReIP	M1	81.78	81.33	80.89	81
	M2	83.64	77.57	79.95	78.36
	M3	82.59	81.11	82.12	82.78

classification results based on classifiers than in that case also linear SVM gives the best classification accuracy which is followed by ensemble bagged trees, ensemble boosted trees and medium *k*NN. In case of M3, which is a holdout validation approach. It shows that the ensemble boosted trees gives the classification accuracy better than other classifiers which is then followed by linear SVM, ensemble bagged trees and medium *k*NN.

From all the experimental results, we have found that method 2 gives the highest classification accuracy of 83.64% by using linear SVM. Thus, we can say that for the classification of images from ISIC 2016 dataset, our ReIP gives best results by extracting relevant information. Comparative analysis of all the obtained results using various feature descriptors with 4 different classifiers is given in Table 7. According to Al-masni et al. [7], the classification accuracies achieved by them using Inception-v3, ResNet-50, Inception-ResNet-v2, and DenseNet-201 are 77.04%, 79.95%, 81.79%, and 81.27% for ISIC 2016 dataset which are less than our proposed method. Along with this, we have also compared our results with the methods proposed by Satheesha et al. [39] and Mahbod et al. [24] by using ISBI2016_ISIC_Part3_Test_Data for testing and ISBI2016_ISIC_Part3_Training_Data for training. Confusion matrices of obtained results are shown in Figure 12 and the values of precision, recall and accuracies of all the three methods

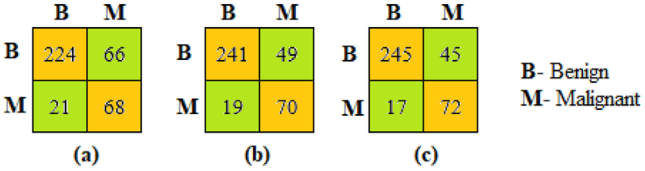

FIGURE 12 Confusion matrices obtained after classifying images in ISBI2016_ISIC_Part3_Test_Data test dataset by using (a) Satheesha et al.'s [39], (b) Mahbod et al.'s [24] and (c) ReIP methods

TABLE 8 Comparative analysis of proposed method with previous methods on ISBI2016_ISIC_Part3_Test_Data test dataset

Method	Precision	Recall	Accuracy
Satheesha et al. [39]	91.42	77.24	77.04
Mahbod et al. [24]	92.69	83.10	82.05
ReIP	93.51	84.48	83.64

are indicated in Table 8. Thus, we can say that our method is also giving better results over deep learning methods.

7 | CONCLUSION

The aim of this paper is to develop a new feature extraction method known as regional information pattern (ReIP) for the classification of skin cancer lesions. In the field of computer vision and machine learning several methods have been developed which have shown their importance specially LBP feature descriptor. Nowadays, deep learning methods have taken the place of machine learning algorithms for getting better results. However, many problems have been faced by these methods such as unavailability of high performance computer with powerful graphical processing units and taking a large amount of time to extract features from the image. Therefore, here, we have tried to bridge these gaps and proposed feature extraction method which can extract relevant features from the image in very less time and can work with normal machine learning algorithms. ReIP has shown extremely better performance over others in all the experiments which we have conducted in order to show its effectiveness. In the field of medical image analysis, the system which gives highly accurate results in less time is preferred over others for early treatment of patients as day by day large number of patients come to hospitals for their timely treatment. Thus, use of ReIP can be beneficial in providing better treatment to the patients.

ORCID

Anjali Gautam https://orcid.org/0000-0003-2675-4073

REFERENCES

1. Globocan 2018: India factsheet. http://cancerindia.org.in/globocan-2018-india-factsheet/ (2020). Accessed 15 May 2020
2. Global solar UV index - a practical guide. https://www.who.int/uv/publications/en/UVIGuide.pdf?ua=1. Accessed 4 March 2021
3. Radiation: Ultraviolet (UV) radiation and skin cancer. https://www.who.int/uv/faq/skincancer/en/index1.html (2020). Accessed 1 May 2020
4. Ultraviolet (UV) radiation. https://www.cancer.org/cancer/cancer-causes/radiation-exposure/uv-radiation.html (2020). Accessed 1 May 2020
5. Akram, T. et al.: Skin lesion segmentation and recognition using multichannel saliency estimation and M-SVM on selected serially fused features. J. Ambient Intell. Hum. Comput. 1–20 (2018) .https://doi.org/10.1007/s12652-018-1051-5
6. Al-Masni, M.A., et al.: Skin lesion segmentation in dermoscopy images via deep full resolution convolutional networks. Comput. Methods Programs Biomed. 162, 221–231 (2018)
7. Al-Masni, M.A., Kim, D.H., Kim, T.S.: Multiple skin lesions diagnostics via integrated deep convolutional networks for segmentation and classification. Comput. Methods Programs Biomed. 190, 105351 (2020)
8. Argenziano, G., et al.: Accuracy in melanoma detection: a 10-year multicenter survey. Journal of the American Academy of Dermatology 67(1), 54–59 (2012)
9. Dash, M., et al.: PsLSNet: Automated psoriasis skin lesion segmentation using modified U-Net-based fully convolutional network. Biomed. Signal Process. Control 52, 226–237 (2019)
10. Dubey, S., Singh, S., Singh, R.: Local diagonal extrema pattern: a new and efficient feature descriptor for ct image retrieval. IEEE Signal Process Lett. 22(9), 1215–1219 (2015)
11. Dubey, S., Singh, S., Singh, R.: Local wavelet pattern: a new feature descriptor for image retrieval in medical ct databases. IEEE Trans. Image Process. 24(12), 5892–5903 (2015)
12. Dubey, S.R.: Local directional relation pattern for unconstrained and robust face retrieval. Multimedia Tools and Applications 78(19), 28063–28088 (2019)
13. Gautam, A., Raman, B.: Local gradient of gradient pattern: a robust image descriptor for the classification of brain strokes from computed tomography images. Pattern Analysis and Applications 23, 797–817 (2020)
14. Gautam, A., Raman, B.: Skin cancer classification from dermoscopic images using feature extraction methods. In: IEEE Region 10 Conference (TENCON), pp. 958–963. Osaka (2020)
15. Ghalejoogh, G.S., Kordy, H.M., Ebrahimi, F.: A hierarchical structure based on stacking approach for skin lesion classification. Expert Syst. Appl. 145, 113127 (2020)
16. Guo, Z., Zhang, L., Zhang, D.: A completed modeling of local binary pattern operator for texture classification. IEEE Trans. Image Process. 19(6), 1657–1663 (2010)
17. Gutman, D. et al.: Skin lesion analysis toward melanoma detection: a challenge at the International Symposium on Biomedical Imaging (ISBI) 2016, hosted by the International Skin Imaging Collaboration (ISIC). https://arxiv.org/abs/1605.01397 (2016)
18. Healsmith, M., et al.: An evaluation of the revised seven-point checklist for the early diagnosis of cutaneous malignant melanoma. British Journal of Dermatology 130(1), 48–50 (1994)
19. Jafari, M.H., et al.: Extraction of skin lesions from non-dermoscopic images for surgical excision of melanoma. International journal of computer assisted radiology and surgery 12(6), 1021–1030 (2017)
20. Jerant, A.F., et al.: Early detection and treatment of skin cancer. American family physician 62(2), 357–368 (2000)
21. Kadampur, M.A., Al Riyaee, S.: Skin cancer detection: applying a deep learning based model driven architecture in the cloud for classifying dermal cell images. Inf. Med. Unlocked 18, 100282 (2020)
22. Kasmi, R., Mokrani, K.: Classification of malignant melanoma and benign skin lesions: implementation of automatic abcd rule. IET Image Proc. 10(6), 448–455 (2016)
23. Li, H., et al.: Dense deconvolutional network for skin lesion segmentation. IEEE J. Biomed. Health. Inf. 23(2), 527–537 (2018)
24. Mahbod, A., et al.: Fusing fine-tuned deep features for skin lesion classification. Computerized Medical Imaging and Graphics 71, 19–29 (2019)
25. Mahbod, A., et al.: The effects of skin lesion segmentation on the performance of dermatoscopic image classification. Comput. Methods Programs Biomed. 197, 105725 (2020)
26. Marchetti, M.A., et al.: Results of the 2016 International Skin Imaging Collaboration International Symposium on Biomedical Imaging Challenge: comparison of the accuracy of computer algorithms to dermatologists for the diagnosis of melanoma from dermoscopic images. Journal of the American Academy of Dermatology 78(2), 270–277 (2018)
27. Masood, A., Ali Al-Jumaily, A.: Computer aided diagnostic support system for skin cancer: a review of techniques and algorithms. Int. J. Biomed. Imaging 2013, (2013)
28. Menegola, A. et al.: Knowledge transfer for melanoma screening with deep learning. In: IEEE 14th International Symposium on Biomedical Imaging (ISBI 2017), Melbourne (2017)
29. Menzies, S.W., et al.: Dermoscopic evaluation of nodular melanoma. JAMA dermatology 149(6), 699–709 (2013)
30. Moh'd Shamaileh, A., et al.: A new feature-based wavelet completed local ternary pattern (Feat-WCLTP) for texture image classification. IEEE Access 8, 28276–28288 (2020)

31. Ojala, T., Pietikäinen, M., Harwood, D.: A comparative study of texture measures with classification based on featured distributions. Pattern Recognit. 29(1), 51–59 (1996)
32. Ojala, T., Pietikainen, M., Maenpaa, T.: Multiresolution gray-scale and rotation invariant texture classification with local binary patterns. IEEE Trans. Pattern Anal. Mach. Intell. 24(7), 971–987 (2002)
33. Otsu, N.: A threshold selection method from gray-level histograms. IEEE Trans. Syst. Man Cybern. 9(1), 62–66 (1979)
34. Pour, M.P., Seker, H.: Transform domain representation-driven convolutional neural networks for skin lesion segmentation. Expert Syst. Appl. 144, 113129 (2020)
35. Premaladha, J., Ravichandran, K.: Novel approaches for diagnosing melanoma skin lesions through supervised and deep learning algorithms. Journal of medical systems 40(4), 96 (2016)
36. Rassem, T.H., Khoo, B.E.: Completed local ternary pattern for rotation invariant texture classification. Sci. World J. 2014, (2014)
37. Rigel, D.S., et al.: ABCDE—an evolving concept in the early detection of melanoma. Archives of dermatology 141(8), 1032–1034 (2005)
38. Sadri, A.R., et al.: WN-based approach to melanoma diagnosis from dermoscopy images. IET Image Proc. 11(7), 475–482 (2017)
39. Satheesha, T., et al.: Melanoma is skin deep: a 3D reconstruction technique for computerized dermoscopic skin lesion classification. IEEE J. Transl. Eng. Health Med. 5, 1–17 (2017)
40. Schaefer, G., et al.: An ensemble classification approach for melanoma diagnosis. Memetic Computing 6(4), 233–240 (2014)
41. Song, T., et al.: Spatially weighted order binary pattern for color texture classification. Expert Syst. Appl. 147, 113167 (2020)
42. Tan, M., Le, Q.V.: Efficientnet: Rethinking model scaling for convolutional neural networks. arXiv:190511946 (2019)
43. Tan, X., Triggs, B.: Enhanced local texture feature sets for face recognition under difficult lighting conditions. IEEE Trans. Image Process. 19(6), 1635–1650 (2010)
44. Tyagi, A., Mehra, R.: An optimized cnn based intelligent prognostics model for disease prediction and classification from dermoscopy images. Multimedia Tools and Applications 79(35), 26817–26835 (2020)
45. Wu, Y. et al.: Automatic skin lesion segmentation based on supervised learning. In: Seventh International Conference on Image and Graphics, Qingdao (2013)
46. Xie, F., et al.: Melanoma classification on dermoscopy images using a neural network ensemble model. IEEE Trans. Med. Imaging 36(3), 849–858 (2016)
47. Xie, F., et al.: Skin lesion segmentation using high-resolution convolutional neural network. Comput. Methods Programs Biomed. 186, 105241 (2020)
48. Xie, Y., et al.: A mutual bootstrapping model for automated skin lesion segmentation and classification. IEEE Trans. Med. Imaging 39(7), 2482–2493 (2020)
49. Yang, W., Zhang, X., Li, J.: A local multiple patterns feature descriptor for face recognition. Neurocomputing 373, 109–122 (2020)
50. Yuan, Y., Chao, M., Lo, Y.C.: Automatic skin lesion segmentation using deep fully convolutional networks with Jaccard distance. IEEE Trans. Med. Imaging 36(9), 1876–1886 (2017)

How to cite this article: Gautam A, Raman B. Towards accurate classification of skin cancer from dermatology images. *IET Image Process.* 2021;1–16. https://doi.org/10.1049/ipr2.12166